Loosely Coupled Transformer Structure and Interoperability Study for EV Wireless Charging Systems

Wei Zhang, *Student Member, IEEE*, Jeff C. White, Arpith Mathew Abraham, and Chunting Chris Mi, *Fellow, IEEE*

***Abstract*—As the wireless power transfer (WPT) technology has been proved to be a convenient and reliable charging method to plug-in hybrid electric vehicles and electric vehicles, the loosely coupled transformer structure and size are the primary and fundamental concern to design an efficient WPT system. In this paper, a double D (DD) coil and a unipolar coil are selected to conduct the study. We focus on the coil structure design to achieve the maximum coupling coefficient as well as efficiency with two situations: 1) with no misalignment, and 2) with a 75-mm door-to-door and 100-mm front-to-back misalignment at which the maximum operating capability can still be achieved. A coil size optimization process is proposed for both the DD coil and the unipolar coil configurations. The relationship between the size of the secondary (receiving) coil, which determines the weight of the pad on the vehicle, and achievable maximum efficiency is studied for both coil topologies. The interoperability between the two coil topologies is studied. The proposed transformer structures with aluminum shielding meet human exposure regulations of the International Commission on Non-Ionizing Radiation Protection guidelines as a foundation. Finally, experiments validated the analyses.**

***Index Terms*—Electric vehicle (EV), electromagnetic radiation, interoperability, loosely coupled transformer, safety, wireless power transfer (WPT).**

I. Introduction

ELECTRIC vehicles (EV) and plug-in hybrid electric vehicles (PHEV) provide superior energy efficiency while offering an enormous potential for reducing CO_2 emissions. Plug-in charging of EVs and PHEVs is still the premier choice since the conductive charging is the traditional method to transfer power. With the development of wireless power transfer (WPT) technology in the past two decades, it becomes possible to charge the vehicles without the physical contact. It is unnecessary to plug or unplug the charging cable, resulting in prevention of electric shock to the operator. The vehicle can be recharged wirelessly and automatically and is not affected by weather conditions, since the primary and secondary coils can be embedded into safety cases.

Manuscript received October 6, 2014; revised April 4, 2015; accepted May 11, 2015. Date of publication May 14, 2015; date of current version July 10, 2015. Recommended for publication by Associate Editor S. Y. Hui.

W. Zhang and C. C. Mi are with the Department of Electrical and Computer Engineering, University of Michigan-Dearborn, Dearborn, MI 48188 USA (e-mail: w.zhang112@gmail.com; chrismi@umich.edu).

J. C. White and A. M. Abraham are with DENSO International America, Inc., Soufield, MI 48188 USA (e-mail: jeff_c_white@denso-diam.com).

Color versions of one or more of the figures in this paper are available online at http://ieeexplore.ieee.org.

Digital Object Identifier 10.1109/TPEL.2015.2433678

Different types of technologies are proposed for wireless power transmission [1]–[3]. Magnetic resonance or mid-range WPT [3]–[5], operating at high-frequency band (3–30 MHz), has the power transfer distance up to several meters [3]. However, it is hard to provide power level as high as 3.3 kW or above, which is normally the power level for a private EV charging, with reasonable size, cost, and good energy transmission efficiency. Therefore, short-range WPT or inductive power transfer is widely used in wireless charging to home appliance [6], [7], EVs [8]–[11], implantable devices [12], [13], etc. Since its operating frequency is selected at relatively low-frequency and very low frequency (VLF) band (3–300 kHz) [2], the power rating for short-range WPT systems covers tens of milliwatts in biomedical applications [14], to several kilowatts or several tens of kilowatts in EV applications [11]. The distance of power transmission for short-range WPT technology, which is usually less than the magnetic resonance technology, ranges from millimeters to hundreds of millimeters. In this paper, the short-range WPT technology is selected and studied for an EV charging application.

The key challenge of the WPT technology is its lower transfer efficiency and lower pickup power than the conductive power transmission [15]. It is caused by multiple reasons and the most immediate cause is its low coupling coefficient (k) of the loosely coupled transformer adapted in the WPT system. The leakage magnetic flux has a lower reluctance path through the large air gap between the primary and secondary coils [16], leading to a weak coupling. Generally, the coupling coefficient is proportional to the size of the loosely coupled transformer at a fixed air gap. However, the secondary coil installed on the chassis of an EV is considered as small and as light as possible. And since the primary (sending) coil is installed in the garage or beneath the parking lot surface, its size and weight are not considered as a major concern. This paper begins with the primary coil size optimization to achieve the maximum coupling coefficient with the secondary (receiving) coil diameter fixed. The purpose is to design a WPT system with a desirable efficiency with the minimum size of the secondary coil.

Two popular coil topologies, double D (DD) and unipolar coils with the shape of a rectangle (including square), are studied in this paper [9], [16]–[18]. The sketch of these two coil types is shown in Fig. 1. Since either the primary or the secondary coil can use a DD or a unipolar coil, the maximum coupling coefficient of these two coil topologies with the same secondary coil area is compared. In addition, automotive manufacturers may select different coil topologies when WPT technology

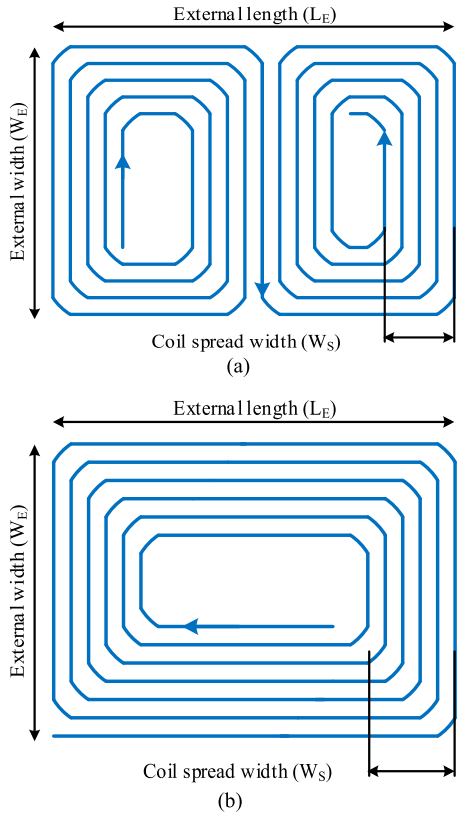

Fig. 1. Coil topologies of loosely coupled transformer. (a) DD coil and (b) unipolar coil topologies.

is commercialized. The interoperability between the two coil topologies is important; therefore, the interoperability between the DD and unipolar coils is studied. Electromagnetic field (EMF) safety of the designed coil is simulated and verified by experiment.

II. Coupling-Related Parameters

As shown in Fig. 1, for each side of coil, there are three parameters determining the coil size: external length (L_E), external width (W_E), and coil spread width (W_S). In this paper, the secondary coil external diameter (L_{E_Sec} and W_{E_Sec}) is fixed, while the other four parameters, $\mathrm{W}_{S\_\mathrm{Sec}}$, $\mathrm{L}_{E\_\mathrm{Pri}}$, $\mathrm{W}_{E\_\mathrm{Pri}}$, and $\mathrm{W}_{S\_\mathrm{Pri}}$, are optimized to achieve the maximum coupling coefficient for this fixed secondary coil size. The tailing subscript_Sec or _Pri indicates the secondary coil or primary coil, respectively. Besides these four variable parameters, other dimensions such as the coil wire diameter, the thickness of the ferrite, the size of the shielding, etc., also have impact on the coupling coefficient. Before the coil size optimization, these coupling-related parameters will be studied and fixed in this section. Since the coupling-related parameters have the similar coupling impact to DD coil and unipolar coil, we use unipolar coil for the study in this section.

The dimensions of a unipolar coil are listed in Table I as the fixed size. Based on this coil size, simulations are conducted to find the influence of the coupling-related parameters to coupling coefficient. The research is conducted by finite element analysis

TABLE I
Simulation Parameters in Section II

Unipolar coil size		Values (mm)
Secondary coil	L_{E_Sec}	250
	W_{E_Sec}	250
	W_{S_Sec}	50
Primary coil	L_{E_Pri}	450
	W_{E_Pri}	450
	W_{S_Pri}	240
Air gap		150
Vehicle chassis size		1200 × 1200
Coupling-related parameters		**Values**
Coil	Coil layer thickness	1 to 15 mm
	Space between turns	0.1 to 2 mm
Ferrite Material permeability		1 to 3000
Shielding	Primary shielding size	0 × 0 to 1000 × 1000 mm
	Secondary shielding size	0 × 0 to 1000 × 1000 mm
	thickness	1 to 5 mm
	Distance between the chassis and back-plate to the secondary pad (D_S)	0 to 100 mm

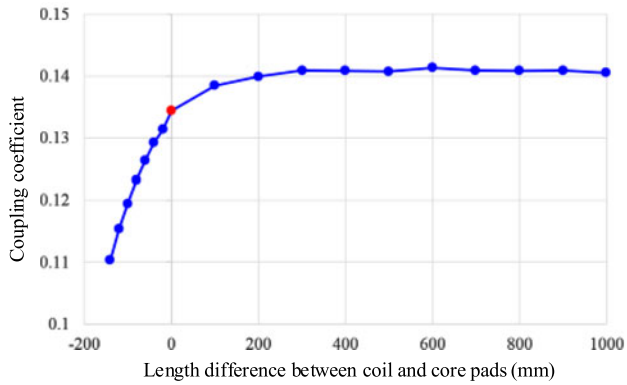

Fig. 2. Coupling coefficient versus the length difference between coil and magnetic core pads.

(FEA) software—Maxwell and HFSS from ANSYS, Inc. All simulations are conducted with a percentage error of 1%. The coupling-related parameters in Table I are studied in this section and can be applicable to both DD and unipolar coil topologies.

A. Magnetic Core

The simulation is first conducted by using a whole plate of ferrites as the magnetic core in both primary and secondary sides with a relative permeability of 2000. According to the simulation result in Fig. 2, a higher coupling coefficient can be achieved by adapting a larger size of the core pad than the coil pad. However, the increase is not significant (less than 0.01) compared to the scenario that the sizes of core and coil pads are the same. Therefore, we select the size of magnetic core pad to be the same as the external diameter of the coil pad in the following simulation.

Ferrite bars are widely used in WPT designs to make a tradeoff between the weight and coupling coefficient [9]. As shown in Fig. 3, different numbers of ferrite bars for the unipolar coil in

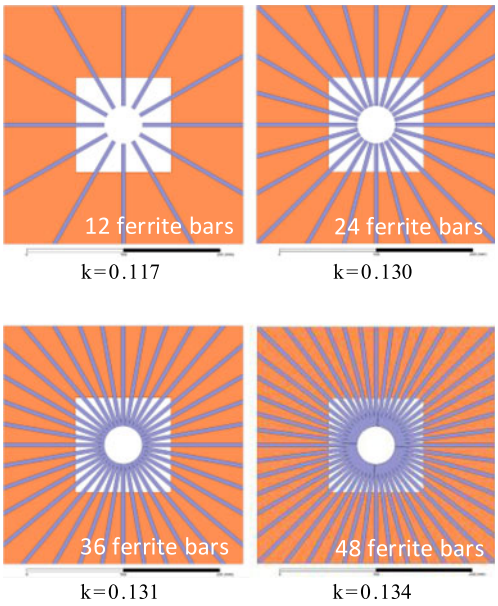

Fig. 3. Coupling coefficient of magnetic bars. For comparison, the value of k without using any ferrite is 0.079, and the value of k using a magnetic plate is 0.136.

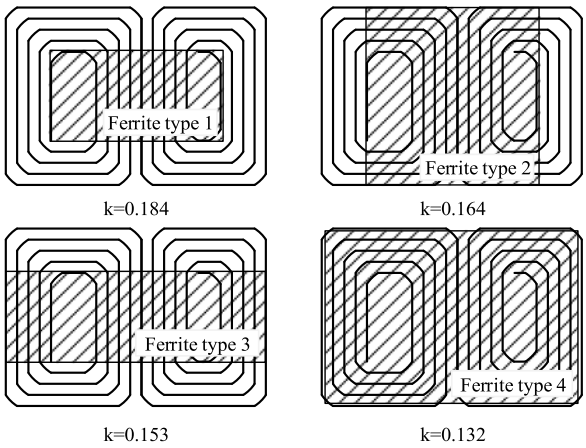

Fig. 4. Coupling coefficient of different ferrite types of a DD coil.

Table I are simulated to compare with the value of k of a whole ferrite plate. Simulation results (shown in Fig. 3) suggest that the number of bars is directly related to the value of coupling coefficient. The larger the number of the ferrite bars, the higher k it can achieve; a magnetic plate can achieve higher coupling coefficient than bars. However, the value of k is not linear with the number of bars and has limited increase when using more than 24 bars. In the following simulation, a magnetic plate is selected for simplification of modeling and simulation.

However, the shape of magnetic plate for a unipolar coil and a DD coil should be different. For a unipolar coil, according to simulation result, larger magnetic plate size can achieve higher k value. Therefore, the magnetic plate of a unipolar coil is selected as the same size of the coil ($L_E \times W_E$). For a DD coil, four types of ferrite plates as shown in Fig. 4 are simulated and

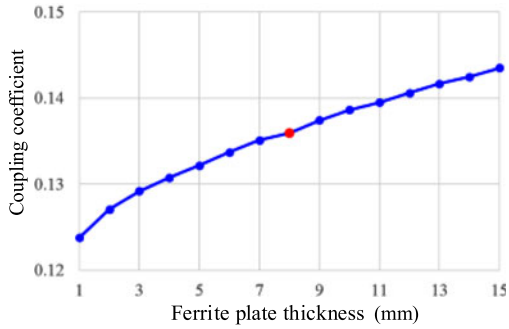

Fig. 5. Coupling coefficient versus ferrite plate thickness.

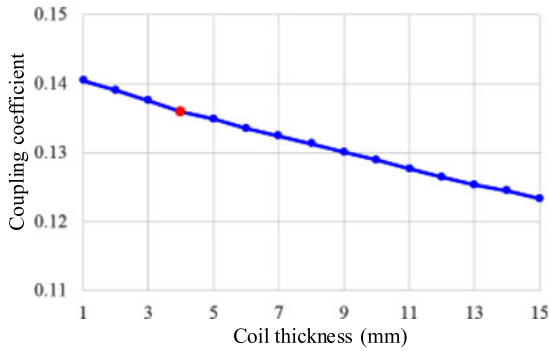

Fig. 6. Coupling coefficient versus coil layer thickness.

compared for better coupling. In the simulation, the size of the DD coil has the same secondary coil area as the unipolar coil in Table I, and simulation is conducted according to the process in Section III. According to the simulated k values in Fig. 4, ferrite type 1 has the best k and is adapted in the following sections.

The simulation results of coupling coefficient versus the magnetic plate thickness are shown in Fig. 5. A thicker layer of ferrite leads to a higher coupling coefficient. We select 8 mm as the thickness of the magnetic plate. In practice, the ferrite thickness should be selected not only considering light weight but according to the magnetic flux density of the power level, to make sure the ferrite material does not saturate at the maximum power output.

B. Coil

The simplified coil model that has one turn and one layer is adapted in the simulation. By using this simplification, the mesh triangles in doing the simulation are significantly reduced, but the accuracy is good enough for engineering [19].

The thickness of the coil layer is decided by two parameters, 1) litz wire diameter, which should be selected by the current of the coil, and 2) the number of turns, which should be designed by the mutual inductance or the required power output. Therefore, in the simulation, the coil layer thickness is varied from 1 to 15 mm to verify its influence on the coupling coefficient. The simulation results in Fig. 6 show that k has a linear drop as the coil layer thickness increases. The reason can be explained that when the coil thickness increases, the distance between the

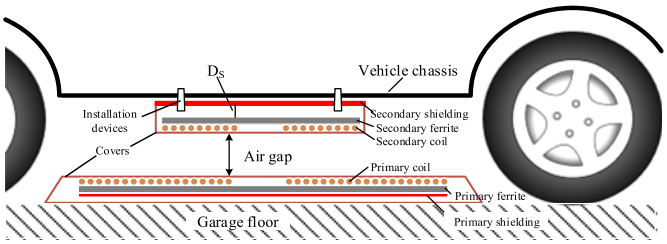

Fig. 7. Diagram of wireless charging platform to vehicles.

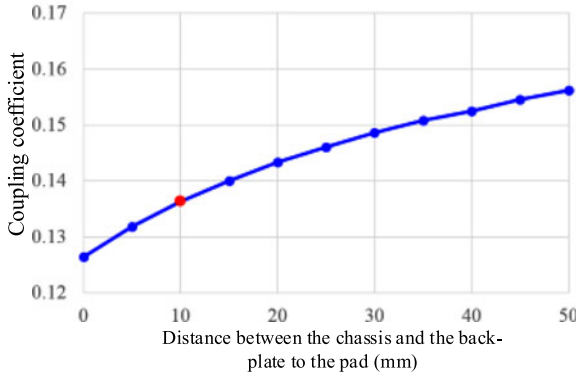

Fig. 8. Coupling coefficient versus the distance between chassis and the back-plate to the pad.

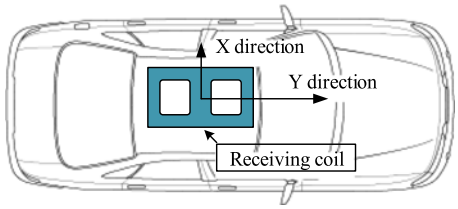

Fig. 9. Demonstration of misalignment directions.

ferrites in the primary and secondary increases, which leads to a lower *k*. In the following studies, we select 4 mm as the coil thickness for the following simulations.

The space between wires influences the coupling since the leakage flux tends to directly close from the wire spaces. Simulation is conducted for variable wire spaces while keeping the coil diameter W_S constant, by changing the wire diameter and the number of turns. The simulation results suggest that smaller wire space leads to a higher coupling coefficient. A similar study for low-power WPT system is reported in [20]. Therefore, zero wire space is used in the simulation. In practice, we can spread the litz wire strands in one layer to make sure the space between the turns is as small as possible.

C. Shielding and Vehicle Chassis

A charging platform diagram is depicted in Fig. 7, in which the secondary coil is installed in the center of the vehicle chassis. To study the coupling coefficient, we use a metal plate with the size of 1200 $\times$ 1200 mm to replace the vehicle chassis in the simulation. Since this metal plate size is large enough compared with the size of the secondary coil, it has almost the same effect as the real vehicle chassis, but a smaller size than the actual vehicle can save more time in running the simulations.

Usually, aluminum shielding is added to both the primary and secondary coils. The shielding in the primary is to block the magnetic flux from going down to the metal bars below the floorboard of the garage to cause eddy current loss. The shielding in the secondary is to prevent the magnetic flux from entering the vehicle chassis (iron) and causing losses and to protect human sitting inside the vehicle. Simulation results indicate that a larger size aluminum shielding results in a lower coupling. The shielding size is fixed to be the same as the coil size.

The simulation results also show that the distance D_S between the chassis and the back-plate to the pad has great impact on the coupling coefficient. In the secondary side, the simulation results suggest that the impact of this distance (D_S) is much more obvious than that of the primary side. The coupling coefficient versus the distance between the secondary shielding and the secondary ferrite is plotted in Fig. 8. For practical consideration, we select the value of 10 mm for D_S. In this 10-mm gap, power converter components can be integrated, cooling system can be designed to help dissipating heat and fix the coil package installation structures of the secondary coil on the bottom of the vehicle, etc.

For the thickness of the aluminum shielding plate, since in the FEA simulation, the shielding is regarded as a perfect electric boundary, the shielding thickness has little influence to the coupling coefficient. Therefore, we select 1 mm as the shielding thickness in the simulation.

III. Structure Design for No Misalignment

Misalignment may happen when the vehicle is parked for charging. In this paper, the maximum X-direction misalignment (door-to-door, or right-to-left) distance is set as 100 mm, and the Y-direction misalignment (front-to-rear) is set as 150 mm (see Fig. 9). Since the output power and efficiency will drop when misalignment happens, methods and structures are proposed to improve tolerance to misalignment and to handle the variations in coupling and power.

Since the diameter of the secondary coil is fixed, one method for a larger misalignment tolerance is to increase the area of the primary coil, which is discussed in Section IV.

Multiple primary coil or multiple secondary coil is studied in [8] and [19]. When misalignment happens, an alternative coil can be used to transfer power. This method is effective to improve the tolerance. However, since the position detection technique and more complicated circuit design as well as control method are required, it will add complexity and significant cost to the system. Another method, by using movable primary coil, will totally eliminate the misalignment problem [21]. By using position detection and mechanical movable devices, the position of the primary coil can be changed to cancel the misalignment.

In this section, we focus on the situation when there is no misalignment. For both DD and unipolar coil topologies, the

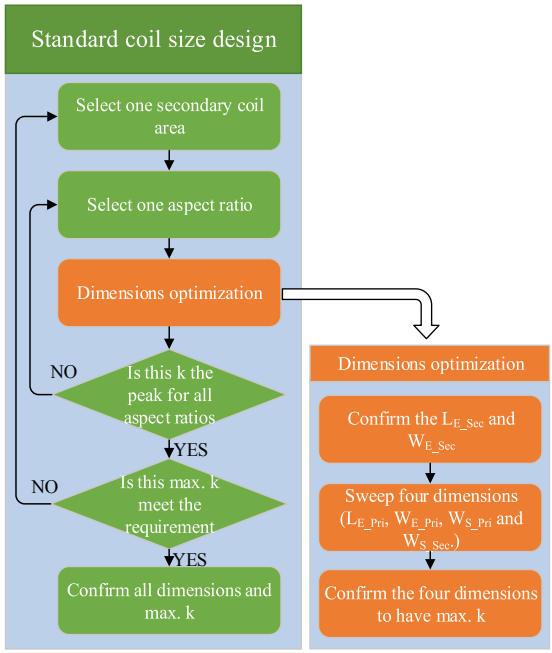

Fig. 10. Flowchart of coil size optimization for maximum *k*.

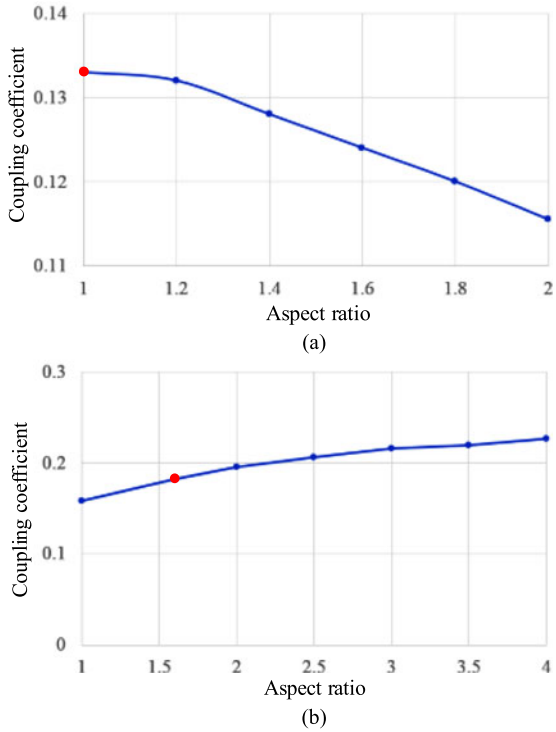

Fig. 11. Coupling coefficient versus the aspect ratio of (a) unipolar coil and (b) DD coil.

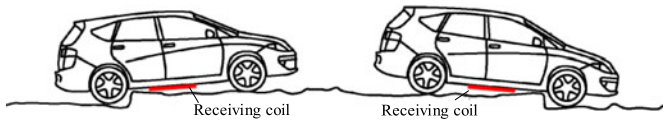

Fig. 12. Demonstration of the large coil aspect ratio influence [21].

first step of the structure design is to confirm the aspect ratio—length/width ratio of the secondary coil. The situation with maximum allowable misalignment will be studied in the following section.

A. Aspect Ratio

To optimize the aspect ratio and compare the maximum couplings between the two types of coils, we should make sure that the secondary coil area is constant. Therefore, we select the rectangle unipolar to compare with the DD coil. The secondary coils of the two topologies have the same coil area of 625 cm^2 (250 mm $\times$ 250 mm).

In the simulation, other coupling-related parameters are selected as stated in Section II. The simulation process is conducted as shown in Fig. 10. For the fixed secondary coil area of 625 cm^2, first select the aspect ratio as 1. Therefore, the secondary coil diameter L_{E_Sec} and W_{E_Sec} are both 250 mm. Change the four coil parameters, W_{S_Sec}, L_{E_Pri}, W_{E_Pri}, and W_{E_Pri}; by parametric sweep simulation, a group of optimized parameters and the maximum *k* for aspect ratio 1 can be achieved. Then we vary the coil aspect ratio from 1 to 4. By comparing the highest coupling coefficient, we can find the best aspect ratio.

The maximum coupling coefficient versus the aspect ratio for both coil topologies is shown in Fig. 11. For a unipolar coil, it has the maximum coupling coefficient when the aspect ratio equals 1. For a DD coil, coupling coefficient gets higher with the aspect ratio increases. This is because the magnetic field has different distributions for the DD and unipolar coil types. Unipolar coils utilize the magnetic field in both *X*- and *Y*-directions; the optimized coil shape is a square, while for the DD coil, the magnetic flux going through the two poles (in the *Y*-direction) has contribution to the coupling coefficient; therefore, a larger aspect ratio can be a better solution. However, a too large aspect ratio may cause the receiving coil installed on the bottom of the vehicle getting damaged when the vehicle runs through a bump as shown in Fig. 12. Therefore, we select the aspect ratio of 1.6:1 for the following research.

B. Comparison of Square and Circular Unipolar Coils

For the unipolar coil topology, a square coil and a circular coil having the similar magnetic field distribution are compared. The simulations are conducted to compare the maximum *k* for these two shapes with the same secondary coil area. For the secondary square coil with $L_{E\_\mathrm{Sec}} = W_{E\_\mathrm{Sec}} = 250$ mm, the maximum k is 0.136, when the primary coil size is 450 $\times$ 450 mm. The area of its primary coil is 2025 cm^2. According to the simulation result of the circular coil, when the secondary coil radius is 141 mm (same coil area of 625 cm^2), the maximum *k* reaches 0.135 when the primary coil radius is 250 mm, which has an area of 1963 cm^2. Therefore, the square and circular coils are almost identical and the coil area to have maximum *k* is approximately equal to each other. The difference may be caused by the parametric sweep step of 20 mm.

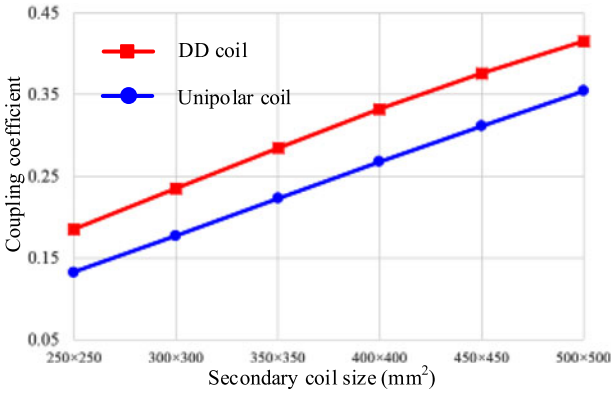

Fig. 13. Coupling coefficient versus secondary coil area.

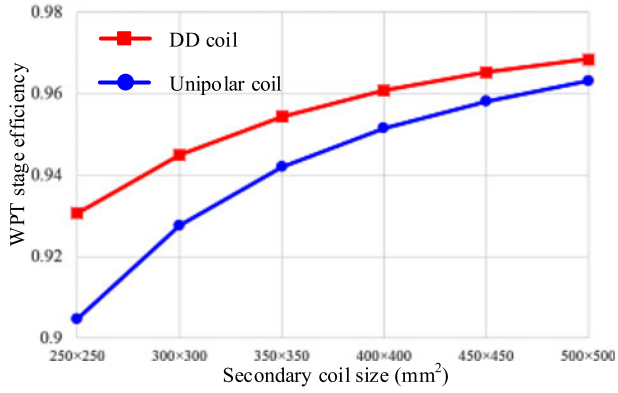

Fig. 14. WPT stage efficiency versus secondary coil size.

C. Maximum Coupling Coefficient and Efficiency of Variable Secondary Coil Size

For the secondary coil size 250 mm × 250 mm, we have analyzed the aspect ratio and the achievable maximum *k*. In this part, the simulation of different coil sizes for both the DD and unipolar coil types is conducted. The aspect ratio of the DD and unipolar coils are selected as 1.6 and 1, respectively.

Fig. 13 shows the simulation result of variable secondary coil sizes. The *k* improvement with size is almost linear. The simulation results suggest that the DD coil is better in coupling by comparison with the same secondary size of a unipolar coil. However, a DD coil needs a larger size of primary coil to achieve a higher *k*. For instance, a 250 mm × 250 mm unipolar coil needs the primary coil size to be 450 mm × 450 mm to get the maximum k of 0.136, while for a DD coil, the optimized primary coil has the size of 460 mm × 740 mm to have *k* of 0.184. The detailed secondary and primary coil sizes can be found in the Appendix. From Fig. 13 and the Appendix, we can make the selection of the desirable coupling coefficient with the consideration of both the secondary and primary pad sizes. The coupling coefficient can be even better by improving the other coupling-related parameters, such as increasing the distance D_S.

For a WPT system with series compensation in both primary and secondary, the maximum power transmission efficiency can be expressed as [22], [23]

$$\eta_{\max} = \frac{\alpha}{\left(1+\sqrt{1+\alpha}\right)^2} \tag{1}$$

$$\alpha = k^2 \cdot Q_{\mathrm{Peq}} \cdot Q_{\mathrm{Seq}} \tag{2}$$

where $\eta_{\max}$ is decided by the coupling coefficient and the winding quality factors. For a loosely coupled transformer with magnetic cores, the power loss on the magnetic material should also be included for efficiency calculation. Usually, the quality factor of the loosely coupled transformer coils can reach 200.

Also considering the ESR of the compensation capacitors and equivalent resistance of the power switches of the inverters, conservatively, we select $Q_{\mathrm{Peq}} = Q_{\mathrm{Seq}} = 150$ for system efficiency calculation, and the result is shown in Fig. 14. The $\eta_{\max}$ can be different if the selections of litz wire and ferrite material are changed; however, it will keep the same trend of the curve.

The efficiency curves in Fig. 14 are no longer linear as the *k* curves in Fig. 13. When the value of coupling coefficient is relatively small, the improvement of coupling can achieve more improvement in efficiency. However, when it increases to a certain value, the improvement of coupling will give limited increase of efficiency since the winding quality factor dominates the system's efficiency.

IV. Structure Design for Misalignment

The relationship between the maximum coupling coefficient and the size of the coil is studied in this section when misalignment happens. First, for the coil sizes designed in Section III, misalignment simulation is conducted. The misaligned *k* value is shown in Fig. 15.

The coupling coefficient has about 50% drop when the worst misalignment happens. According to the simulation, the DD coil has a better coupling coefficient than the unipolar coil with misalignment, which is caused by its larger primary coil size.

The primary coil size designed in Section III is optimized for maximum *k* at no misalignment. However, a maximum operating capability (MOC) to output full power at a certain misalignment distance should be required. In this paper, the MOC misalignment distance is set as 75 mm in X-direction, and 100 mm in Y-direction. The output power is related to the value of *k*. Taking the primary *LCC* secondary series compensation topology as an example [24], the output voltage can be expressed as

$$V_{\mathrm{out}} = kV_{\mathrm{in}}\frac{\sqrt{L_P L_S}}{L_{RP}} \tag{3}$$

where L_P and L_S are the primary and secondary coil inductances, and L_{RP} is the series-connected resonant inductance in the primary. Therefore, the output power will drop when misalignment occurs.

If the designed coil size cannot meet the MOC misalignment requirement, according to Fig. 15, increasing the secondary coil size is a possible solution. In this section, coil size is redesigned to have the maximum *k* at the MOC misalignment position instead of the design to have maximum *k* with no misalignment.

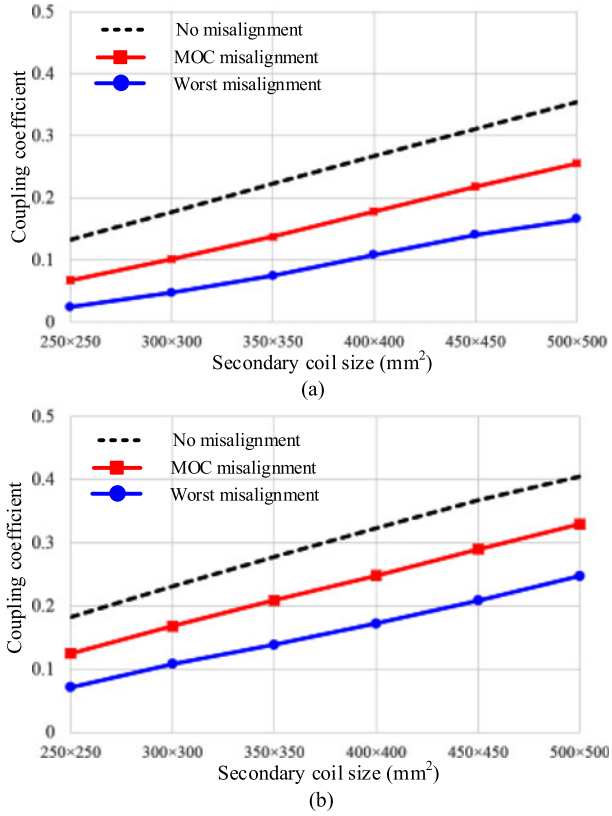

Fig. 15. Coupling coefficient versus secondary coil size of (a) unipolar coil and (b) DD coil. This size is designed with the original purpose to have maximum k at no misalignment.

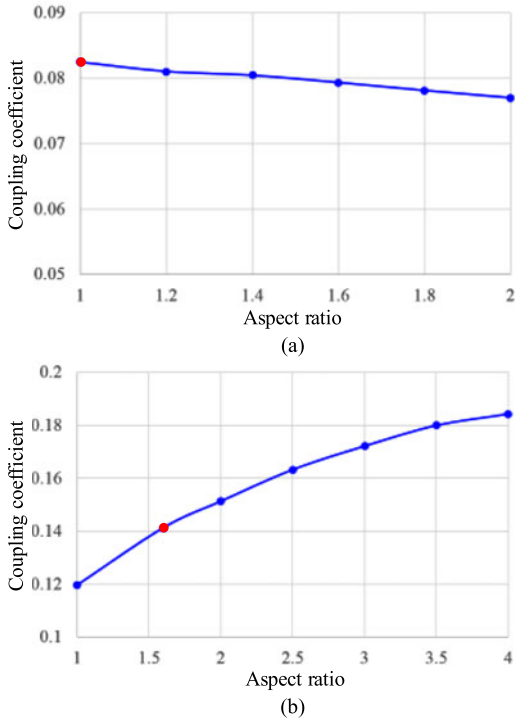

Fig. 16. Coupling coefficient versus the aspect ratio of (a) unipolar coil and (b) DD coil at the MOC misalignment.

The secondary coil has the same L_{E_Sec} and W_{E_Sec} values as in Section III, but is set at the MOC misalignment position. The four coil parameters, W_{S_Sec}, L_{E_Pri}, W_{E_Pri}, and W_{E_Pri}, are redesigned according to the process in Fig. 10 to optimize the aspect ratio and the value of k. Therefore, the redesign in this section guarantees that the maximum k is achieved at the MOC misalignment.

Fig. 16 shows the coupling coefficient versus aspect ratio of the unipolar and DD coils. Similar to the no misalignment scenario in Section III, when the aspect ratio of a unipolar coil equals one, it has the maximum coupling. Therefore, different sizes of unipolar secondary coils are simulated by using aspect ratio of one. The simulation result is depicted in Fig. 17(a). This design is the optimized size for the MOC misalignment; therefore, compared with the results in Fig. 15(a), the misalignment coupling coefficient especially at the MOC misalignment is improved, while the value of k drops when there is no misalignment. In addition, this design has the primary coil size larger than the no misalignment design in Section III. For instance, for a 250 × 250 mm secondary coil, the optimized primary coil size in Section III is 450 × 450 mm, while for the design in this section, the required primary coil size is 620 × 650 mm.

For the DD coil topology, the same design process is conducted. The coupling coefficient keeps increasing with a reasonable aspect ratio range (from 1 to 4). For the same reason

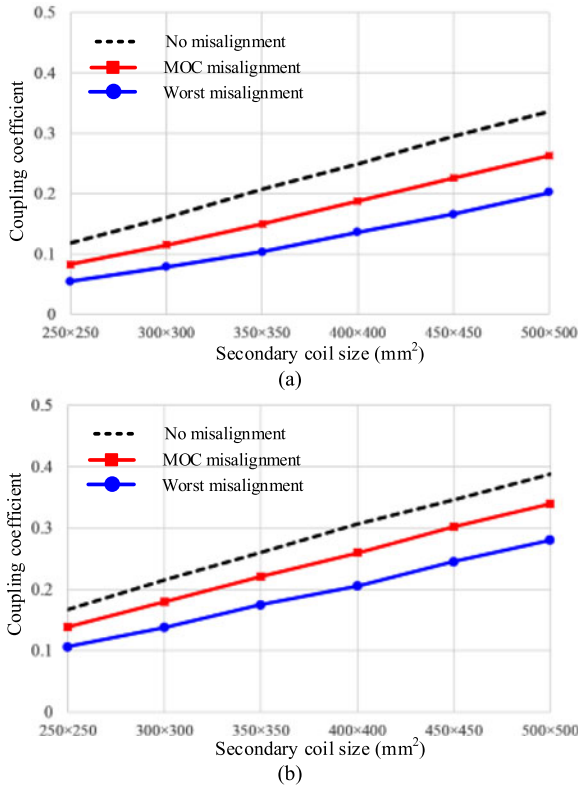

Fig. 17. Coupling coefficient versus secondary coil size of (a) unipolar coil and (b) DD coil. This design is optimized for the maximum k at the MOC misalignment position.

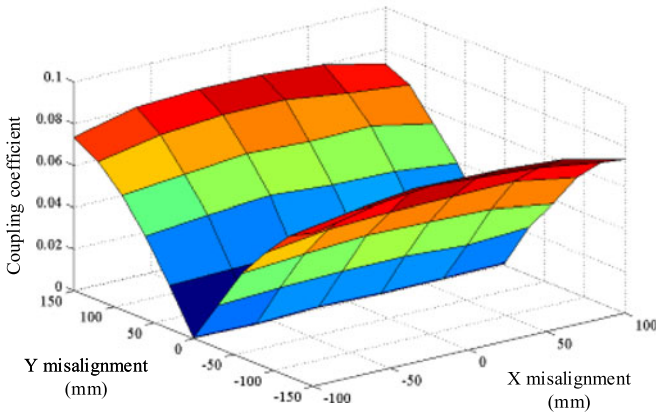

Fig. 18. Interoperable coupling coefficient of unipolar secondary coil and DD primary coil. This figure is an example as the size of secondary coil 250 × 250 mm and primary coil 540 × 760 mm. The primary coil is the optimized size for a 250 × 250 mm secondary DD coil.

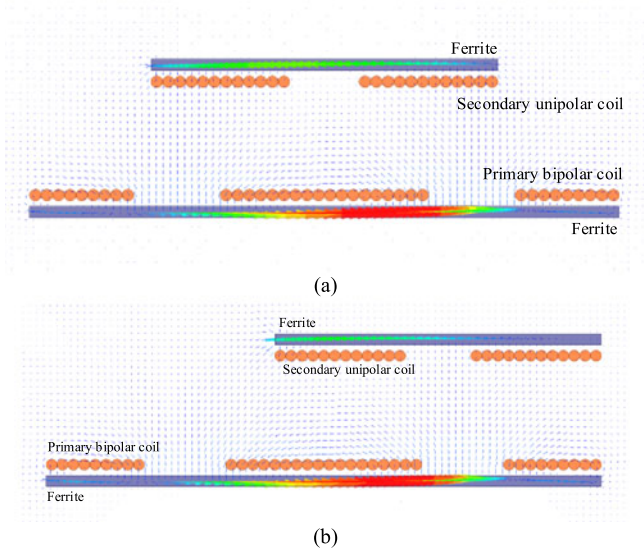

Fig. 19. Sketch to illustrate the magnetic field distribution of interoperability.

mentioned and displayed in Fig. 12, we select the aspect ratio value of 1.6. The redesign result of a DD coil topology is shown in Fig. 17(b). These two coil designs in Sections II and III have advantages in different aspects; designers can make their choice according to Figs. 15 and 17 to make sure both system efficiency and MOC requirements are met.

V. Interoperability

WPT devices will be manufactured by different equipment manufacturers, which may use different types of coils. Therefore, interoperability between the DD and unipolar coils should be studied to ensure the primary and secondary coils will work together seamlessly. The optimized coil size with no misalignment in section III is used to study the interoperability problem. Other designs with variable coil sizes should have similar results since the magnetic field distribution is the same.

If the secondary adapts a unipolar coil topology, while a DD coil is installed in the primary side, the coupling coefficient simulation result in the full misalignment area is shown in Fig. 18.

The coupling coefficient is zero when there is no *Y*-direction misalignment as shown in Fig. 18. This can be explained that for the primary DD coil, the magnetic flux goes from one pole to the other, as displayed in Fig. 19(a). The flux goes in and out of the secondary unipolar coil; therefore, the total magnetic flux is zero. In the secondary coil area, no magnetic linkage as well as no induced voltage across the coil. This situation gets improved when the *Y*-direction misalignment happens. From Fig. 19(b), it can be recognized that the in and out magnetic flux gets imbalanced due to *Y*-direction misalignment. This imbalance is maximized when the *Y* has the worst misalignment. Therefore, the interoperable maximum *k* appears at the worst *Y* misalignment.

The values of *k* versus misalignment tendency is almost identical when the primary and secondary coils are unipolar and DD, respectively. The maximum interoperable coupling coefficients (at 150-mm *Y* misalignment and 0-mm *X* misalignment) are listed in Table II for different sizes of coils. The primary and secondary coils are selected as the optimized sizes designed in Section III. For convenience of comparison, the percentage drop of coupling coefficient is labeled behind the interoperation values compare with the situation of the same secondary coil topology. The value of *k* for the primary-DD and secondary-unipolar interoperation has approximately 50% drop at the maximum *Y* misalignment position. While the value of *k* for the primary-unipolar and secondary-DD interoperation drops less than 25% and drops less when the size gets smaller. For the secondary DD coil of 198 mm × 316 mm and primary unipolar coil of 450 mm × 450 mm, the coupling drop is only 6.8%.

TABLE II
Interoperation Coupling Coefficient of Variable Coil Size

Secondary coil size (mm^2)	Pri. unipolar.—sec. DD (percentage drop)	Pri. DD—sec. unipolar (percentage drop)
250 × 250	0.124 (6.8%)	0.082 (56%)
300 × 300	0.162 (8.8%)	0.105 (55%)
350 × 350	0.193 (14%)	0.136 (52%)
400 × 400	0.219 (18%)	0.169 (49%)
450 × 450	0.247 (21%)	0.190 (49%)
500 × 500	0.265 (25%)	0.208 (50%)

VI. Safety

The EMF generated by WPT systems may induce high field strength in the body tissue of humans, implanted devices, living organisms nearby, etc. This raises the important safety issues of the whole body heat stress, excessive localized tissue heating, and adverse health effects. The EMF radiation should comply with the international safety guidelines. International Commission on Non-Ionizing Radiation Protection (ICNIRP) regulations have been established to limit human exposure to time-varying EMF with the aim of preventing adverse health effects. The guidelines provide reference safety restrictions of

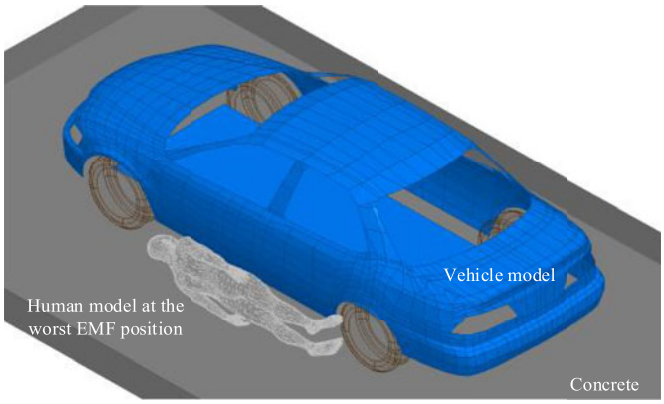

Fig. 20. Simulation models for radiation.

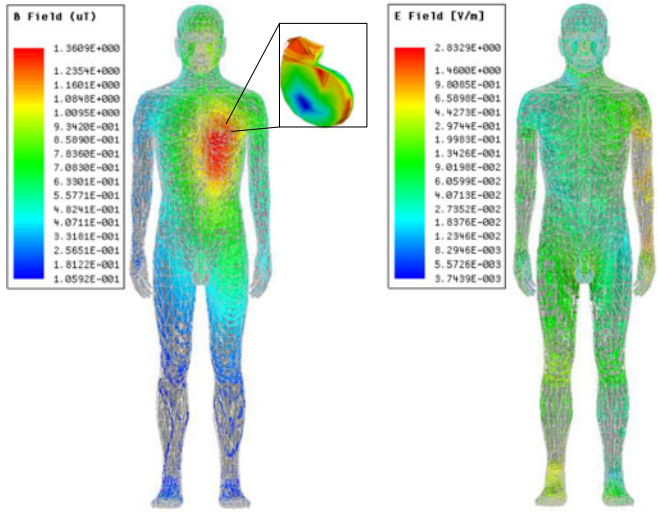

Fig. 21. Simulation results of magnetic field and electric field for the worst case.

both electric field and magnetic field for occupational exposure and general public exposure.

The ICNIRP stipulates the limitations for general public should not be exposed to body average RMS flux densities greater than 27 μT in the frequency range of 3 kHz to 10 MHz. The limit is raised for occupational exposure to 100 μT. The electric field limitations for the general public is 83 V/m, for occupational exposure is 170 V/m [25].

A detailed anatomical human model with 14 internal organs as well as a titanium pacemaker provided by DENSO International America, Inc., is used for the numerical simulations in this paper. A cat model is used to test the radiation level when this small animal goes under the vehicle. The vehicle is also modeled, because the vehicle body, especially its chassis has shielding effect to magnetic field since the material is metal. The car glasses and all objects inside, which are not metal and far from the radiation source, are neglected.

The worst case to have the highest level of radiation (average in the chest and heart area) is the human laying down at his left side, face the vehicle and the radiation source as shown in Fig. 20, since at this position the distance between the pacemaker and the loosely coupled transformer is the closest. The worst case for the animal is the cat laying down just between the primary and secondary of the transformer with no misalignment.

A 3.3-kW WPT system is designed and simulated for EMF radiation. All the circuit specifications can be found in Section VII. In the simulation, the RMS currents on the primary and secondary coils are 7.49 and 13.10 A, respectively. The phase angle between the primary and secondary current is set at 85° (supported by the measurement in Section VII). The simulation result of the worst EMF position is shown in Fig. 21 for the unipolar coil without misalignment. The left chest of the human body has the maximum magnetic field value, while the maximum electric field value appears at the left armpit, which has the shape edge of the simulated human model. However, the worst electric and magnetic fields are both well below the ICNIRP regulations even at the worst misalignment position. The detailed radiation values are listed in Table III.

The simulation is also conducted for the small animal laying down in between the charging pads, and the magnetic field strength is shown in Fig. 22. Since the cat is laying down on the ground by its left side, the maximum magnetic field appears at its left side stomach, and the value is 2.68 mT. This radiation level is much higher than the regulations for human. There is still no radiation limit for animals; however, it is not considered as safe for animals below the vehicle. Foreign object detection system is needed to protect small animals.

TABLE III
SIMULATION RESULTS OF THE WORST RADIATION POSITION

Coil position	Magnetic field (μT)		Electric field (V·m^{-1})	
	Max. on tissue	Max. on pacemaker	Max. on tissue	Max. on pacemaker
No misalignment	1.36	1.02	2.83	0.33
Worst misalignment	2.48	1.76	2.81	0.38

VII. EXPERIMENT VERIFICATION

A unipolar circular loosely coupled transformer prototype as shown in Fig. 23 is built to verify the analysis. In order to trade-off between system efficiency and coil size, the secondary coil diameter is selected as 300 mm. According to the coil optimization process, the primary coil external diameter is optimized as 600 mm and has the maximum coupling coefficient of 0.184. We use ferrite bars in the simulation and experiment instead of magnetic plate since it is easily available and light weight. The loosely coupled transformer information can be found in Table IV. The measured coupling coefficient is 0.182, which is close to the simulated value. The simulated and measured k values with misalignment are shown in Fig. 25.

We design the circuit with the primary *LCC* and secondary *LCC* compensation as shown in Fig. 24 [26]. The detailed circuit specifications are listed in Table V. Circuit parameters are designed for nonmisalignment scenario. The detailed circuit design process is not described in this paper. The system power

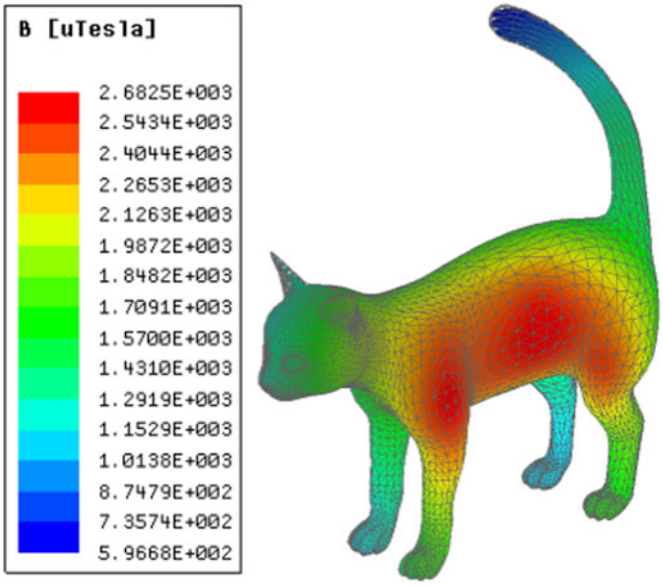

Fig. 22. Simulation results of magnetic field for small animals laying inside the air gap of the loosely coupled transformer.

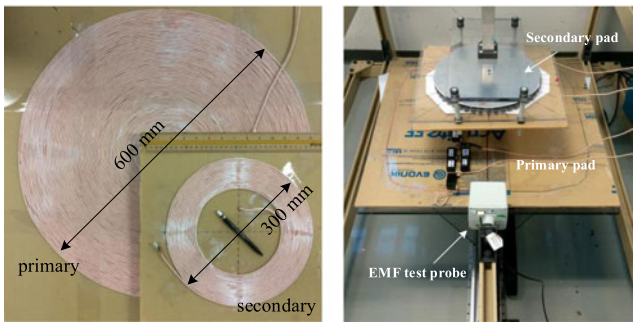

Fig. 23. Loosely coupled transformer prototype.

TABLE IV
PROTOTYPE LOOSELY COUPLED TRANSFORMER

Coil parameters		Specifications
Coil topology		Unipolar
Coil	Primary	32 turns, litz wire with 800 strands AWG38, no gap between wires
	Secondary	16 turns, litz wire with 800 strands AWG38, two wires connected in parallel as one turn, no gap between wires
Core	Primary	48 bars of PC40 with 8-mm thickness, same external diameter with the primary coil.
	Secondary	48 bars of PC40 with 8-mm thickness, same external diameter with the secondary coil.
Shieldings		2-mm aluminum circular sheet, same size with the coil
Air gap		150 mm

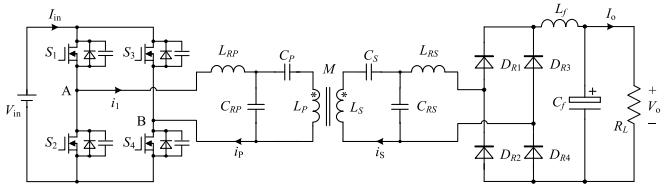

Fig. 24. *LCC–LCC* circuit diagram for experimentation.

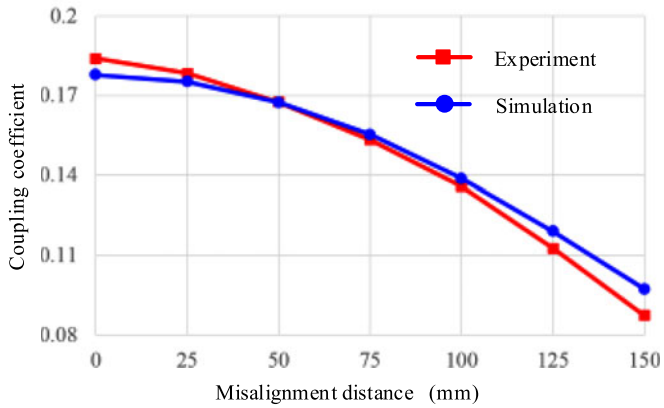

Fig. 25. Coupling coefficient versus misalignment distance.

TABLE V
CIRCULAR SPECIFICATIONS OF UNIPOLAR COIL TYPE WITH NO MISALIGNMENT

Parameters	Value
Output power	3.3 kW
Battery voltage	400 V
Output voltage	408.7 V
Input voltage	350 V
Operating frequency	85 kHz
L_P	420 μH
L_S	110 μH
Coupling coefficient	0.182
L_{RP}	62 μH
L_{RS}	43 μH
C_{RP}	54.6 nF
C_{RS}	84.2 nF
C_P	9.02 nF
C_S	42.67 nF

level and operating frequency is selected according to a technic information report of J2954 by Society of Automotive Engineers (SAE) [27], [28].

The experiment result is shown in Fig. 26. The system efficiency is affected by the distance D_S between the chassis and the back-plate to the secondary pad. As in the coupling simulation, this D_S value impacts the value of k and therefore influence the system efficiency. Without the secondary shielding plate, the system efficiency reaches 93.6% and drops to 92.6% if D_S is 5 mm.

For the 100-mm misalignment distance, the input voltage has to increase to 442 V to guarantee the 3.3-kW output. In addition, at the 150-mm misalignment distance, since the input voltage

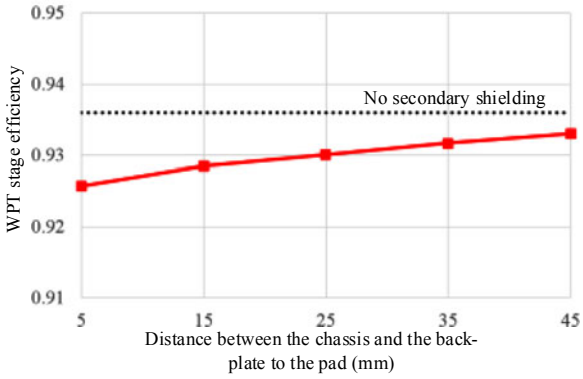

Fig. 26. System efficiency versus distance between the chassis and the back-plate to the secondary pad.

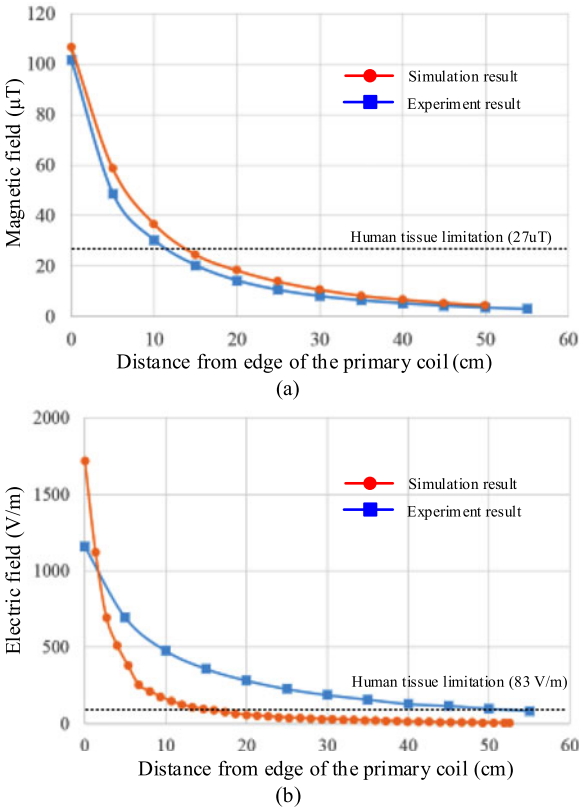

Fig. 27. Simulated and measured result of (a) magnetic field and (b) electric field.

is designed to have the limitation of 450 V, the system can only achieve 1.8-kW power output, and the system efficiency drops to 88%.

EMF is measured with an electric and magnetic field probe EHP-200 (frequency ranges from 9 kHz up to 30 MHz) along the line midway between the pads. The line begins from the edge of the primary coil. The measured and simulated results along this line are shown in Fig. 27, with ICNIRP exposure limits for general public plotted. The spot flux density is 27.3 μT at a distance of 140 mm from the primary pad edge, while the electric field density requires human stands 500 mm away from the primary pad edge. The electric field drops faster within a few centimeters from 0 cm. Since the probe is a cube with a size of 85 mm $\times$ 85 mm $\times$ 89 mm, and the system is not measured in an electromagnetic shielding chamber, it may cause inaccuracy of the measurement especially the electric field near 0 cm, as seen from Fig. 27(b).

TABLE VI
SIZE AND MAXIMUM COUPLING COEFFICIENT OF UNIPOLAR AND DD COILS

Coil types	Secondary coil size (mm)			Primary coil size (mm)			Max. k
	L_{E_Sec}	W_{E_Sec}	W_{S_Sec}	L_{E_Pri}	W_{E_Pri}	W_{S_Pri}	
Unipolar	250	250	88	450	450	203	0.136
	300	300	105	500	500	225	0.178
	350	350	123	550	550	248	0.223
	400	400	140	570	570	252	0.268
	450	450	158	620	620	293	0.311
	500	500	175	650	650	312	0.355
DD	198	316	24	460	740	130	0.185
	237	379	28	480	770	135	0.235
	277	443	44	500	800	140	0.285
	316	506	51	510	830	125	0.332
	356	569	71	550	850	149	0.376
	395	632	79	580	880	176	0.415

VIII. CONCLUSION

This paper provides the optimized sizes of the unipolar and DD type loose coupled transformer for wireless EV chargers. The coil sizes are designed to have the maximum coupling coefficient and efficiency. The achievable maximum efficiency is linear with the size of the secondary coil pad. The loosely coupled transformer can be designed either for the maximum k of no misalignment or the maximum k at the required worst case misalignment to have the MOC. The simulation results and data can be directly applied to EV and PHEV WPT systems. The Interoperability problem is studied when the primary and secondary pads have different coil types. Radiations of both magnetic and electric fields are conducted for safety considerations. It shows that a safe system can be designed for human; however, approaches should be adopted for small animals which go under the vehicle. The experimental result validated the analytical result.

APPENDIX

The detailed dimensions of both the primary and secondary of the loosely coupled transformer is listed in Table VI. The unipolar and DD coils have the aspect ratio of 1 and 1.6, respectively. The design is optimized for maximum k at no misalignment position.

REFERENCES

[1] S. Y. R. Hui, Z. Wenxing, and C. K. Lee, "A critical review of recent progress in mid-range wireless power transfer," *IEEE Trans. Power Electron.*, vol. 29, no. 9, pp. 4500–4511, Sep. 2014.
[2] G. A. Covic and J. T. Boys, "Inductive power transfer," *Proc. IEEE*, vol. 101, no. 6, pp. 1276–1289, Jun. 2013.

[3] J. Garnica, R. A. Chinga, and L. Jenshan, "Wireless power transmission: From far field to near field," *Proc. IEEE*, vol. 101, no. 6, pp. 1321–1331, Jun. 2013.
[4] M. Kiani and M. Ghovanloo, "The circuit theory behind coupled-mode magnetic resonance-based wireless power transmission," *IEEE Trans. Circuits Syst. I, Reg. Papers*, vol. 59, no. 9, pp. 2065–2074, Sep. 2012.
[5] P. Jongmin, T. Youndo, K. Yoongoo, K. Youngwook, and N. Sangwook, "Investigation of adaptive matching methods for near-field wireless power transfer," *IEEE Trans. Antennas Propag.*, vol. 59, no. 5, pp. 1769–1773, May 2011.
[6] S. Y. R. Hui, "Planar wireless charging technology for portable electronic products and Qi," *Proc. IEEE*, vol. 101, no. 6, pp. 1290–1301, Jun. 2013.
[7] S. Y. R. Hui and W. W. C. Ho, "A new generation of universal contactless Battery charging platform for portable consumer electronic equipment," *IEEE Trans. Power Electron.*, vol. 20, no. 3, pp. 620–627, May 2005.
[8] M. Budhia, J. T. Boys, G. A. Covic, and H. Chang-Yu, "Development of a single-sided flux magnetic coupler for electric vehicle IPT charging systems," *IEEE Trans. Ind. Electron.*, vol. 60, no. 1, pp. 318–328, Jan. 2013.
[9] M. Budhia, G. A. Covic, and J. T. Boys, "Design and optimization of circular magnetic structures for lumped inductive power transfer systems," *IEEE Trans. Power Electron.*, vol. 26, no. 11, pp. 3096–3108, Nov. 2011.
[10] G. A. Covic and J. T. Boys, "Modern trends in inductive power transfer for transportation applications," *IEEE J. Emerging Sel. Topics Power Electron.*, vol. 1, no. 1, pp. 28–41, Mar. 2013.
[11] K. Jiseong, K. Jonghoon, K. Sunkyu, K. Hongseok, S. In-Soo, S. Nam Pyo, D.-H. Cho, J. Kim, and S. Ahn, "Coil design and shielding methods for a magnetic resonant wireless power transfer system," *Proc. IEEE*, vol. 101, no. 6, pp. 1332–1342, Jun. 2013.
[12] Q. Chen, S. C. Wong, C. K. Tse, and X. Ruan, "Analysis, design, and control of a transcutaneous power regulator for artificial hearts," *IEEE Trans. Biomed. Circuits Syst.*, vol. 3, no. 1, pp. 23–31, Feb. 2009.
[13] G. B. Joung and B. H. Cho, "An energy transmission system for an artificial heart using leakage inductance compensation of transcutaneous transformer," *IEEE Trans. Power Electron.*, vol. 13, no. 6, pp. 1013–1022, Nov. 1998.
[14] F. Sato, T. Nomoto, G. Kano, H. Matsuki, and T. Sato, "A new contactless power-signal transmission device for implanted functional electrical stimulation (FES)," *IEEE Trans. Magn.*, vol. 40, no. 4, pp. 2964–2966, Jul. 2004.
[15] E. Waffenschmidt and T. Staring, "Limitation of inductive power transfer for consumer applications," in *Proc. 13th Eur. Conf. Power Electron. Appl.*, 2009, pp. 1–10.
[16] W. Zhang, Q. Chen, S. C. Wong, C. K. Tse, and X. Ruan, "A novel transformer for contactless energy transmission systems," in *Proc. IEEE Energy Convers. Congr. Expo.*, 2009, pp. 3218–3224.
[17] C. Fernandez, O. Garcia, R. Prieto, J. A. Cobos, S. Gabriels, and G. Van Der Borght, "Design issues of a core-less transformer for a contactless application," in *Proc. Appl. Power Electron. Conf. Expo.*, 2002, pp. 339–345.
[18] A. Zaheer, H. Hao, G. A. Covic, and D. Kacprzak, "Investigation of multiple decoupled coil primary pad topologies in lumped IPT systems for interoperable electric vehicle charging," *IEEE Trans. Power Electron.*, vol. 30, no. 4, pp. 1937–1955, Apr. 2015.
[19] L. Xun and S. Y. R. Hui, "Equivalent circuit modeling of a multilayer planar winding array structure for use in a universal contactless battery charging platform," *IEEE Trans. Power Electron.*, vol. 22, no. 1, pp. 21–29, Jan. 2007.
[20] X. Ferna, C. ndez, O. Garcia, R. Prieto, J. A. Cobos, S. Gabriels, and G. Van Der Borght, "Design issues of a core-less transformer for a contactless application," in *Proc. 17th Annu. IEEE Appl. Power Electron. Conf. Expo.*, 2002, vol. 1, pp. 339–345.
[21] N. P. C. Hanspeter Widmer and L. Sieber, "Wireless power antenna alignment adjustment system for vehicles," U.S. Patent US20 110 254 503 A1, 2011.
[22] W. Zhang, S. C. Wong, C. K. Tse, and Q. Chen, "Analysis and comparison of secondary series- and parallel-compensated inductive power transfer systems operating for optimal efficiency and load-independent voltage-transfer ratio," *IEEE Trans. Power Electron.*, vol. 29, no. 6, pp. 2979–2990, Jun. 2014.
[23] W. Zhang, S. C. Wong, C. K. Tse, and Q. Chen, "Design for efficiency optimization and voltage controllability of series—Series compensated inductive power transfer systems," *IEEE Trans. Power Electron.*, vol. 29, no. 1, pp. 191–200, Jan. 2014.
[24] Z. Pantic, B. Sanzhong, and S. Lukic, "ZCS LCC-compensated resonant inverter for inductive-power-transfer application," *IEEE Trans. Ind. Electron.*, vol. 58, no. 8, pp. 3500–3510, Aug. 2011.
[25] "ICNIRP guidelines for limiting exposure to time-varying electric, magnetic and electromagnetic fields (1 Hz to 100 kHz)," *Health Phys.*, vol. 99, pp. 818–836, 2010.
[26] S. Li, W. Li, J. Deng, T. D. Nguyen, and C. C. Mi, "A double-sided LCC compensation network and its tuning method for wireless power transfer," *IEEE Trans. Veh. Technol.*, vol. PP, pp. 1–1, 2014. DOI 10.1109/TVT.2014.2347006.
[27] J. Schneider, "SAE J2954 overview and path forward," [Online]. Available: http://www.sae.org/smartgrid/sae-j2954-status_1-2012.pdf.
[28] Wireless charging of electric and plug-in hybrid vehicles, SAE J2954, 2015.

Authors' photographs and biographies not available at the time of publication.